UE Antenna Properties and Their Influence on Massive MIMO System Performance

Bengtsson, Erik; Tufvesson, Fredrik; Edfors, Ove

UE Antenna Properties and Their Influence on Massive MIMO System Performance

Erik L. Bengtsson[1], Fredrik Tufvesson[2], Ove Edfors[2]

[1] Network Technology Lab, Sony Mobile Communications, Lund, Sweden

[2] Dept of Electrical and Information Technology, Lund University, Lund, Sweden

Abstract—**The use of large-scale antenna arrays can bring substantial improvements both in energy and spectral efficiencies. This paper presents an initial study of user equipment (UE) antenna performance based on prototypes for a massive MIMO test bed. Most publications in the massive MIMO area have assumed isotropic or dipole antenna characteristics at the UE side. It is, however, of greatest interest to evaluate the impact of realistic antenna implementations and user loading on such systems. In this study antennas are integrated into realistic UE form factors. Simulations are carried out to evaluate system performance using the UE antenna characteristics measured in a Satimo StarGate 64. Comparisons are made with ideal isotropic un-correlated antennas. The presented UEs are designed for the 3.7 GHz band used by the LuMaMi massive MIMO test bed at Lund University.**

Index Terms— **antenna, measurement, massive MIMO, system performance, channel interaction, antenna pattern.**

I. Introduction

Massive MIMO (MaMi) technology [1] is emerging as one of the major candidates for increasing capacity and efficiency of future wireless communications systems [2]. Recent predictions show that energy efficiency can be increased by several orders of magnitude and spectral efficiency by at least one order of magnitude, under reasonable assumptions on channel behavior and system configurations [3]. Predictions like these have opened up a frenetic research activity in the field. Despite great efforts spent on investigating how efficient MaMi systems should be designed, the terminal perspective has been almost entirely neglected. One reason for this is that most of the new concepts relate directly to the base station and only indirectly to the terminal devices. The terminal designs will, however, to a large extent influence the overall performance of MaMi systems, including how well different MaMi transmission techniques perform under real conditions and how transmission protocols are designed. A notable exception to the base station (BS) focus is [4] where the impact of non-linearities in the UE implementation are studied. The study concludes that HW impairments of the UE limit the achievable capacity as the number of BS antennas grows large.

In contrast to most published studies in the MaMi area, where ideal or omni-directional UE antenna behavior is assumed, we address real UE antenna designs, integrated into commercially available smart phone chassis. The antennas are tuned for operation in the 3.7 GHz band used by the Lund University MaMi (LuMaMi) testbed [5]. The unavoidable user interaction with the integrated antennas in the current and future consumer devices influences performance of the antenna systems as well as of the overall communication system. User loading of the antennas cannot be avoided and it is a challenge to minimize its negative effects on the performance. When channel variations that originate from user-loading of the antenna occur, they are commonly compensated for by means of higher power, which is an inefficient method. From the UE perspective, introducing diversity antennas in the terminals was initially a way to combat performance degradation caused by fading. Higher diversity gains, however, often originate from overlooked loading generated antenna losses. Due to the channel hardening effect antenna diversity should not be necessary in MaMi terminals, but we expect that it can not be avoided in devices where the antennas may be exposed to loading.

II. Approach

While the impact of UE antennas in MaMi systems is a large and complex topic, we start our investigations by performing simulation studies along the lines of multiplexing efficiency as defined in [6]. Multiplexing efficiency is a figure of merit for the combined UE antennas in a MIMO system, under the assumption of isotropic propagation conditions. In [7] the authors developed the concept further to take arbitrary distributions of incoming power into account. In this paper we use this concept and extend it to a full MaMi system with multiple UEs, each having an arbitrary number of antennas. Following [7], and for reasons of tractability, we adopt the Kronecker channel model

$$\boldsymbol{H} = \boldsymbol{R}^{1/2}\boldsymbol{H}_W, \tag{1}$$

where $\boldsymbol{R}$ denotes the UE antenna correlation matrix and $\boldsymbol{H}_W$ is a white, independent and identically distributed (i.i.d.), complex Gaussian channel. It is also, in this first study, assumed that the large BS array has zero antenna correlation. If we in the MaMi context incorporate all UE antennas from different terminals into $\boldsymbol{R}$ and assume zero correlation between antennas on different terminals we get an $N \times N$ correlation matrix

$$\boldsymbol{R} = \begin{pmatrix} \boldsymbol{R}_1 & 0 & \cdots & 0 \\ 0 & \boldsymbol{R}_2 & \cdots & 0 \\ \vdots & \vdots & \ddots & \vdots \\ 0 & 0 & \cdots & \boldsymbol{R}_K \end{pmatrix}, \tag{2}$$

where $\boldsymbol{R}_k$ is the $N_k \times N_k$ correlation matrix for the N_k antennas on UE k and

$$N = \sum_{k=1}^{K} N_k. \tag{3}$$

Here we limit ourselves to one or two antennas per UE, i.e. $N_k = 1$ or 2. For an M antenna BS, $\boldsymbol{H}_W$ is an $N \times M$ matrix. The eigenvalue distribution of $\boldsymbol{H}\boldsymbol{H}^H$ gives an indication of the system performance and we are able to analyze how the system capacity is affected by the individual UE antenna performances. The correlation matrices $\boldsymbol{R}_k$ are calculated by combining measured antenna characteristics with different angular distributions on incoming clusters of multipath components (MPCs). For the ideal case, where there is no correlation between any of the UE antennas, $\boldsymbol{R}$ becomes a diagonal matrix. As an illustration of what happens for other correlation values, we present expected values of the sorted eigenvalues of $\boldsymbol{H}\boldsymbol{H}^H$, for a set-up with a 50-antenna BS and four two-antenna UEs (see Fig. 1). For low antenna correlation, the eigenvalue spread is small and we can expect high system capacity, and the opposite as the antenna correlation grows. Antenna correlation is, as we will show, affected by angular spread (AS), distribution of clusters and channel richness.
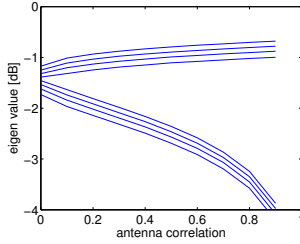

Fig. 1: Impact of pairwise increase of correlation between UE antennas on eigen values.

The exact relation between eigenvalues of $\boldsymbol{H}\boldsymbol{H}^H$ and system performance is non-trivial and can be measured in several ways, which is beyond the scope of this paper. In short, the proposed approach is simplifying the analysis to:

1) concentrating information about UE antenna properties (patterns) and angular distribution of incoming clusters to a single antenna correlation matrix $\boldsymbol{R}_k$ per UE, and
2) that $\boldsymbol{R}_k$ be used in the model (1) to evaluate performance of an entire MaMi system with realistic UE properties. The assumptions enable us to quickly analyze how degraded antenna performance of a single UE, or a number of UEs, influence the entire system. We can also compare different operational modes (diversity vs. spatial multiplexing) for individual UEs.

In the paper we focus on the analysis of UE antenna pairs and spatial multiplexing properties. We concentrate on the limitations seen for the individual antenna configurations, hence $\boldsymbol{R}_k$, and how the antenna performance may impact the performance in a MaMi context. The underlying mechanisms approximated by the model (1) include directional properties of both environment and antennas. In order to more clearly separate antenna and environment influences we use directional descriptions below. To illustrate the difference between MaMi and conventional systems we need to introduce some new measures. To make the investigation manageable we also make some simplifying assumptions that may upper bound the results.

The first assumption is that the MaMi BS is capable of providing phase coherent signals from different clusters of MPCs with individually controlled amplitude to each antenna, here set to unity. The effective gain (EG) and mean effective gain (MEG) of an antenna, for a specific scenario, are both normalized to the performance of an isotropic ideal radiator, for the same scenario. This, however, hides the additional gain available in a MaMi system. Traditionally, diversity or multiplexing gain offered by a channel is obtained in the receiver, as seen in e.g. RAKE and MIMO, and there is no need to include this in the antenna characteristics. In our investigation, however, it is of interest to visualize the additional gain obtained within the channel in order to be able to compare the performance improvements offered by different diversity schemes and antenna configurations. Therefore, we introduce two new measures, the combined coherent gain (CCG) and combined non-coherent gain (CNG). If we assume a cluster of MPCs with an angular spread (AS) illuminating the antenna from an arbitrary angle of arrival (AoA), we can describe the MEG for such a cluster as

$$\rho(\Theta, \Phi, \eta(\Theta, \Phi), A) = \frac{\int_A (\eta(\Theta, \Phi)) dA}{A} \tag{4}$$

where Θ and Φ are elevation and azimuth AoA, respectively, $\eta(\Theta, \Phi)$ is antenna gain at this AoA, and A is an integration area around Θ and Φ defined by the AS. We assume uniform distribution of incoming power over this area. The polar coordinates are defined for $\Phi \in (-\pi, \pi)$ and $\Theta \in (0, \pi)$ with orientation according to Fig. 2. Polarization direction is also defined accordingly, with components along Θ and Φ.
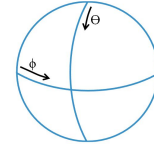

Fig. 2: Orientation of Φ and Θ.

We define CCG as an expectation

$$\text{CCG}(n, A) = \mathrm{E}_{\boldsymbol{\Theta}, \boldsymbol{\Phi}} \left\{ \sum_{i=1}^{n} \rho_i(\Theta_i, \Phi_i, \eta(\Theta_i, \Phi_i), A) \right\} \tag{5}$$

for n clusters with randomly distributed AoAs, all with the same AS. Expectation is over $\boldsymbol{\Theta}, \boldsymbol{\Phi}$, which are vectors collecting the n random AoAs and $\rho_i(\Theta_i, \Phi_i, \eta(\Theta_i, \Phi_i), A)$ is defined in (4). If the AoAs are uniformly distributed over the sphere this equals

$$\text{CCG}(n) = \sum_{i=1}^{n} \rho_{\text{iso}} = n\rho_{\text{iso}}, \tag{6}$$

where ρ_{iso} is the total isotropic efficiency (TE$_{\text{iso}}$) of the antenna. The contribution from each cluster is added in amplitude as we assume coherent contributions from all clusters after massive MIMO pre-coding. For the non coherent case we correspondingly define

$$\text{CNG}(n, \text{A}) = \text{E}_{\boldsymbol{\Theta}, \boldsymbol{\Phi}} \left\{ \sqrt{\sum_{i=1}^{n} \rho_i^2(\Theta_i, \Phi_i, \eta(\Theta_i, \Phi_i), \text{A})} \right\} \quad (7)$$

which, for uniformly distributed AoAs becomes

$$\text{CNG}(n) = \sqrt{\sum_{i=1}^{n} \rho_{\text{iso}}^2} = \sqrt{n}\rho_{\text{iso}}, \quad (8)$$

where we add the power contribution from each cluster, assuming the phase of each contribution to be independent and uniformly distributed over the sphere. The last simplification in both (6) and (8) are possible as the expectation on ρ_{iso} is independent on n. From a simulation perspective we can calculate the expected CCG by means Monte Carlo (MC) simulation and

$$\text{CCG}(n, \text{A}) \approx \frac{\sum_{k=1}^{K} \sum_{i=1}^{n} \rho_i(\Theta_i, \Phi_i, \eta(\Theta_i, \Phi_i), \text{A})}{K}, \quad (9)$$

where n is the number of clusters, K is the number of random realizations of the AoA, and for each k new $\boldsymbol{\Theta}, \boldsymbol{\Phi}$ are generated. As we know that ρ_{iso} has no dependency on n we can make the same simplification as in (6) and (8) also in our simulation, and

$$\text{CCG}(n, \text{A}) \approx \frac{\sum_{k=1}^{K} \left(n \frac{\int_{\text{A}_{\text{tot}}} \eta(\boldsymbol{\Theta}, \boldsymbol{\Phi}) \text{dA}}{\text{A}_{\text{tot}}} \right)}{K} \quad (10)$$

yield the same result as (9) for large K. In (10) we integrate over the combined area, $\text{A}_{\text{tot}} = \cup_{m=1}^{n} \text{A}_m$, of all clusters instead of each individual area, A_m, as in (9). Equations (9) and (10) approach (5) for large K. In our MC simulations we found $K = 2000$ to be sufficient. Expression (10) is useful later in the calculation of multiplexed CCG and multiplexed CNG. The CNG can be estimated as

$$\text{CNG}(n, \text{A}) \approx \frac{\sum_{k=1}^{K} \sqrt{\sum_{n} \rho_i^2(\Theta_i, \Phi_i, \eta(\Theta_i, \Phi_i), \text{A})}}{K}, \quad (11)$$

and similarly

$$\text{CNG}(n, \text{A}) \approx \frac{\sum_{k=1}^{K} \left(\sqrt{n} \frac{\int_{\text{A}_{\text{tot}}} \eta(\boldsymbol{\Theta}, \boldsymbol{\Phi}) \text{dA}}{\text{A}_{\text{tot}}} \right)}{K}. \quad (12)$$

As cluster powers are added in (11), the MEG for the combined area in (12) needs to be multiplied by $\sqrt{n}$. Again (11) and (12) approach (7) as K grows large.

Fig. 3 shows CCG and CNG for an ideal isotropic radiator. For CCG the slope is 3 dB each time the clusters are doubled and for the CNG case it is 1.5 dB. It is noted that CCG and CNG for a single cluster are the same and equals the isotropic total efficiency (TE$_{\text{iso}}$) of the radiator. Looking into combined antenna performance metrics, we assume that the
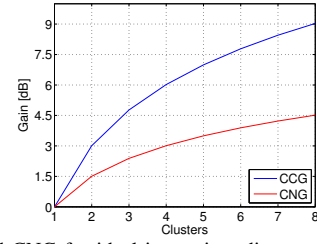

Fig. 3: CCG and CNG for ideal isotropic radiator vs. number of clusters.

transmission channel determines the AoA and that the small spacing between the UE antennas cause the AoA for each cluster to be the same for all the antennas in a UE. Here we introduce an error in directions where antenna pattern correlation is large and gain imbalance is moderate. The results can therefore be seen as upper bounds on what to expect from a real system. A deeper analysis of the magnitude of the deviation is not included as we assume it to be small. For a real system the problem can be solved with zero forcing or other methods to ensure orthogonality. For the squared correlation,

$$\text{ECC}_{\text{A}_{\text{tot}}} = \left| \frac{\int_{\text{A}_{\text{tot}}} (\boldsymbol{E}_1 \cdot \boldsymbol{E}_2) \text{dA}}{\sqrt{\int_{\text{A}_{\text{tot}}} \|\boldsymbol{E}_1\| \text{dA} \int_{\text{A}_{\text{tot}}} \|\boldsymbol{E}_2\| \text{dA}}} \right|^2, \quad (13)$$

where the vector $\boldsymbol{E}_a = [E_{\Theta_a}, E_{\Phi_a}]^T$ contains the complex E-fields for each polarization for antenna a. Integration is performed for the combined area of the multiple clusters, A_{tot} as defined in (10). The $\text{ECC}_{\text{A}_{\text{tot}}}$ can be interpreted as the squared local correlation and we can use it to calculate

$$\text{CCG}_{\text{MPE}} \approx \frac{\sum_{k=1}^{K} n \sqrt{\frac{\int_{\text{A}_{\text{tot}}} (\eta_1) \text{dA}}{\text{A}_{\text{tot}}} \frac{\int_{\text{A}_{\text{tot}}} (\eta_2) \text{dA}}{\text{A}_{\text{tot}}} (1 - \text{ECC}_{\text{A}_{\text{tot}}})}}{K} \quad (14)$$

for high SNRs [6]. This approximation becomes more accurate as K grows. We need to integrate over A_{tot} as the effect of reduced gain imbalance otherwise will be lost when the number of clusters grows larger. Like in (10) we need to multiply each antenna MEG by n, in order to include the effect of coherent amplitude addition of the multiple clusters. For the CNG$_{\text{MPE}}$ the corresponding expression becomes

$$\text{CNG}_{\text{MPE}} \approx \frac{\sum_{k=1}^{K} \sqrt{n \frac{\int_{\text{A}_{\text{tot}}} (\eta_1) \text{dA}}{\text{A}_{\text{tot}}} \frac{\int_{\text{A}_{\text{tot}}} (\eta_2) \text{dA}}{\text{A}_{\text{tot}}} (1 - \text{ECC}_{\text{A}_{\text{tot}}})}}{K}, \quad (15)$$

and, like in (12), we multiply each antenna MEG by $\sqrt{n}$, since the power from each cluster is added. All expressions are defined for linear units while the results are primarily presented in dB. The expected performance of CCG$_{\text{MPE}}$ and CNG$_{\text{MPE}}$ for two uncorrelated ideal isotropic antennas would equal CCG and CNG shown in Fig. 3.

III. ANTENNA EVALUATION RESULTS

For the investigation, five Sony Xperia ZL and Xperia SP chassis have been modified with different antenna configurations. Either with four antennas and circuitry for switching between any antenna pair combination or with two antennas, located at the top and bottom. For the four-antenna prototypes

two antennas are located at the top corners, one at the side and one at the bottom. The TE_{iso} for free space (FS) is similar, about -5 dBi for all 4 antennas, including the loss from the switch circuitry. All antenna configurations have been characterized in a Satimo StarGate 64 measurement facility. 3D patterns for FS, left and right hand (LH/RH), beside head with hand left and right (BHHL/R) have also been measured. The TE_{iso} range over levels from -5 dB down to -14 dB dependent on load scenario. Fig. 4 shows the measured FS antenna E-field patterns for the four-antenna prototype, with ellipses indicating polarization. It can be noted that the patterns for the two top and the side antennas are rather omni-directional, while the bottom antenna shows a directivity downwards. For the two-antenna prototype, the patterns for
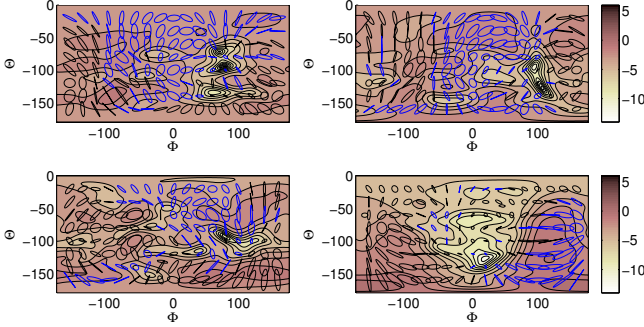

Fig. 4: FS performance for four antenna prototype, upper right, upper left, bottom and side antennas in order. Blue ellipses indicate left hand polarization and black right hand polarization.

both antennas in FS show directivity in different directions and their efficiencies are also quite different. The bottom antenna has a TE_{iso} of -3 dB and the top antenna -4.6 dB.

Fig. 5 shows cumulative distribution functions (CDFs) for E-field patterns for two of the antennas, with different colors for different load scenarios. For each scenario the impact of AS, ranging from 4° to 90° is included as curves with the same color. The load not only decreases the average power by moving the curve to the left but usually also decreases the slope, i.e. directivity which translates to larger variation for different AoA. AS tend to have larger impact when the antennas are loaded and increases the variation even more, i.e. higher probability of low efficiency that may lead to drop outs. The directivity increase is caused by a combination of the hand and head absorption and impact on the current distributions on the radiators. It can also be noted that the slope of the bottom antenna CDF (right) for FS (blue) is less steep compared to the top L antenna (left) already for FS condition. In Fig. 6
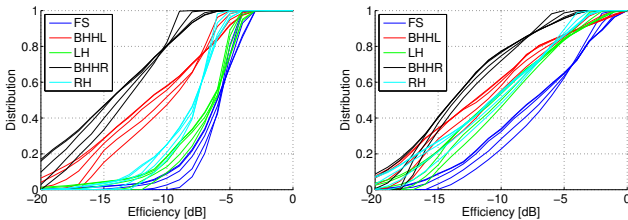

Fig. 5: CDFs of antenna E-field patterns for two of the antennas

we see CCG and CNG vs. number of clusters, which is the

same as Fig. 3 but based on the measured FS patterns from the four-antenna prototype. Performance is plotted with different colors for different antennas. CCG grows almost ideally with about 3 dB per doubling of clusters and CNG with about 1.5 dB. The MaMi gain is obvious but may also translate to faster roll-off when the channel becomes poor. Despite the faster roll-off, the CCG never gets worse than the CNG. The local
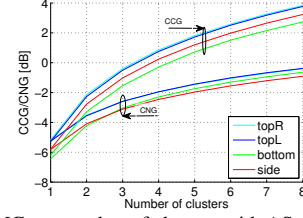

Fig. 6: CCG and CNG vs. number of clusters with AS=4°, for the four antenna prototype in FS.

antenna correlation pattern for a single cluster (n=1), $ECC_{A_{tot}}$, and multiplexed efficiency pattern, CCG_{MPE}, for an AS=4° for the two top antennas on one of the prototypes are shown in the upper part of Fig. 7. Below, the corresponding CDFs for a wider range of AS are shown. Even if the antenna correlation is low in an isotropic environment, the dependency on AS of incoming clusters is substantial and the correlation degrades for a more narrow AS (lower left). The AS also influences the CCG_{MPE}, which is seen as less steep slopes when the AS decreases (lower right). This translates to larger variations and a worse minimum.
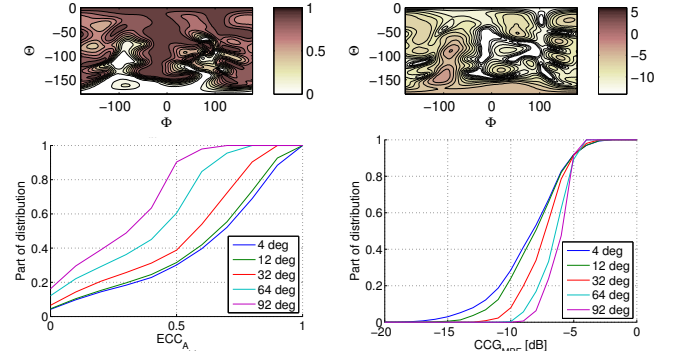

Fig. 7: FS performance for the combination of the top antennas, in terms of $ECC_{A_{tot}}$(n=1) and CCG_{MPE}(n=1) patterns for an AS=4°. Below the corresponding CDFs for a wider range of ASs. The ECC_{iso}=0 and the $CCG_{MPE_{iso}}$=-5.2 dB.

Fig. 8 shows average $ECC_{A_{tot}}$ and average CCG_{MPE}, as defined in (13) and (9), vs. the AS for a single cluster. The figures for FS and BHHL conditions are included for all 6 antenna combinations for the four-antenna prototype. We see low load dependency on $ECC_{A_{tot}}$, except for the combination of top-right and side antenna (indexed TR/S) where the hand probably was close to touching the radiator and obviously affected the current distribution. Larger load dependency on $ECC_{A_{tot}}$ is expected for lower frequencies as the wavelength approaches the size of the prototype and the hand to a larger extent interacts with the current distributions as they to a larger extent are located in the actual grounding structure.

For the CCG_{MPE}, there is an offset based on the efficiency drop. For FS (upper curves), combinations with the bottom antenna (indexed B) have steeper slope due to the higher directivity and this yields larger probability for AoA dependent gain imbalance as the AS gets small. In order to evaluate
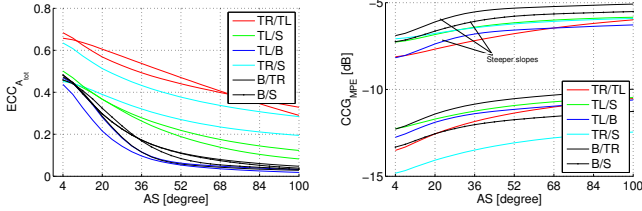

Fig. 8: Average ECC_{MPE} and average CCG_{MPE} for FS and BHHL vs. AS for single cluster.

what happens to the average $ECC_{A_{tot}}$ and average CCG_{MPE} in the different load scenarios, MC simulations of (14) and (15) have been performed where the number of clusters increases from one to eight, with random AoA and all with same AS. Fig. 9 shows the average $ECC_{A_{tot}}$ vs. number of clusters for an antenna pair in the four-antenna prototype. The curves are colored according to load in the left sub-figure and according to AS in the right sub-figure. While for a single antenna combination, the presented $ECC_{A_{tot}}$ are quite representative for any of the antenna combinations and point towards a low load dependency and a strong AS dependency. It can be noted that the $ECC_{A_{tot}}$ converges towards isotropic performance as the number of clusters grows large.
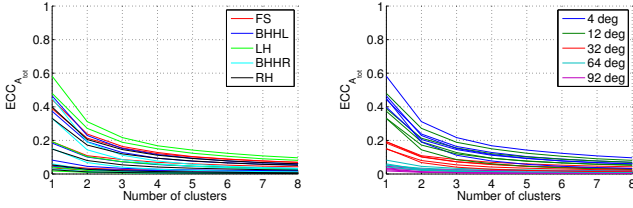

Fig. 9: $ECC_{A_{tot}}$ for one antenna combination of the 4 antennas in the four antenna prototype, vs. clusters, colored vs. load and AS.

The corresponding CCG_{MPE} curves are shown in Fig. 10, colored according to loading in the left sub-figure and according to AS in the right sub-figure. The coloring shows that the dependency on loading is strong, while the dependency on AS is much weaker. The AS dependency is the strongest the fewer the clusters are, seen as a larger spread for few clusters. As CCG_{MPE} is dependent on AS, number of clusters,
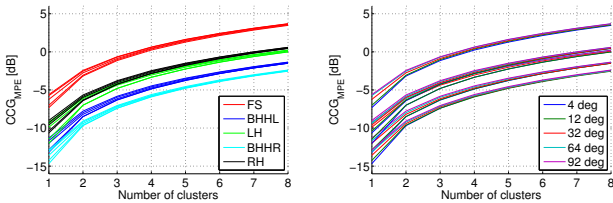

Fig. 10: Typical CCG_{MPE} for an antenna pair vs. number of clusters, coloured vs. AS and vs. load.

and antenna directivity, the slope reaches up to 6 dB going from 1 to 2 clusters for some loading conditions and antenna

combinations. This is to be compared with the expected 3 dB discussed earlier and depicted in Fig. 3. The result may be interpreted as 3 dB comes from doubling the energy and 3 dB from the fact that two clusters are needed for multiplexed operation (rank 2).

IV. SUMMARY AND CONCLUSIONS

Simulations show that the channel in combination with the antenna directional properties have a substantial impact on the performance of a MaMi pre-coded system. Going from a single cluster to two clusters improves CCG_{MPE} significantly more than increasing AS area by a factor of 2 (3 dB vs. 0.1 dB) due to the impact of the gain imbalance and the fact that the two clusters come in from different AoAs. This tells us that even if the BS may be able to improve phase coherence within a narrow cluster of MPCs the impact of gain imbalance at UE side can not be compensated for. The results indicate between 2 and 5 dB of additional drop for single cluster as compared to the isotropic multiplexed efficiency. However, CCG_{MPE} is a rank-two performance indicator and the results simply indicate that we need to switch to rank one, i.e., diversity mode. It can also be mentioned that a design with cross polarized UE antennas would be less sensitive to the channel richness.

For the $ECC_{A_{tot}}$ there is no or very little dependency on load for most antenna combinations while smaller AS and fewer clusters degrade it significantly from the isotropic value (which is zero for all our antenna combinations). What happens with the local correlation, $ECC_{A_{tot}}$, when we go down in frequency is an interesting topic. In this situation the ECC_{iso} is known to vary as current distributions are more affected by user interaction, but the average local correlation may behave differently.

V. ACKNOWLEDGEMENT

REFERENCES

[1] T.L. Marzetta, *"Noncooperative cellular wireless with unlimited numbers of base station antennas*, Wireless Communications, IEEE Transactions on, vol. 9 no.11 pp. 3590-3600, 2010.
[2] E.G. Larsson, F. Tufvesson, O. Edfors, and T.L. Marzetta, *Massive MIMO for Next Generation Wireless Systems*, IEEE Commun. Mag., vol. 52, no. 2, pp. 186-195, Feb. 2014.
[3] H.Q. Ngo, E.G. Larsson, and T.L. Marzetta, *Energy and Spectral Efficiency of Very Large Multiuser MIMO Systems*, IEEE Trans. Commun., vol. 61, no. 4, pp. 1436-1449, Apr. 2013.
[4] E. Björnsson, J. Hoydis, M. Kontouris, M. Debbah, *"Massive MIMO Systems with Non-Ideal Hardware: Energy Efficiency, Estimation, and capacity Limts"* Reviced for resubmission to IEEE Transaction on Information Theory, (available online arxiv.org/abs/1307.2584)
[5] J. Vieira, et al., *A flexible 100-antenna testbed for Massive MIMO*, IEEE International Workshop on Massive MIMO: From theory to practice. Austin, TX, USA, Dec. 2014 (to appear)
[6] R. Tian, B.K. Lau and Z. Ying, *"Multiplexing efficiency of MIMO antennas"* IEEE Antennas Wireless Propagat. Lett., vol. 10, pp. 183-186, 2011.
[7] R. Tian, B.K. Lau and Z. Ying, *"Multiplexing efficiency of MIMO antennas in Arbitrary Propagation scenarios"* 6th European Conference on Antennas and Propagation, (EUCAP), Prague, Czech Republic, Mar. 2012.